

Wetting of TiC and TiN by metals

S. V. Dudiy* and B. I. Lundqvist

Department of Applied Physics, Chalmers University of Technology and Göteborg University, SE-412 96 Göteborg, Sweden

(Received 9 July 2003; revised manuscript received 21 January 2004; published 30 March 2004)

A number of important issues raised by brazing technologies and recent wetting experiments with liquid metals on TiC and TiN are analyzed at the microscopic level, using first-principles density-functional computational experiments. The large variations of the wetting angles for Cu and Ag on TiC and TiN from experiment to experiment are connected to the relative contributions of different local atomic coordinations at the interface. The key factors in the structure dependence of Ag/Ti(C,N) interface energetics are identified, such as the varying number of the metal-C(N) bonds and the strength of metal-Ti bonding. Interface adhesion is shown to be improved by C(N) vacancies, in agreement with observed better wettability of hypostoichiometric carbides. Based on Al/Ti(C,N)(001) and Ti/Ti(C,N)(001) simulations, the effects of Ti and Al interface segregation in the metal melt are estimated. The metal-C(N) bonding across the Cu,Ag,Au/Ti(C,N)(001) interfaces is similar to the metal-enhanced covalent bonding previously reported for Co/Ti(C,N)(001) and Co/WC(001). The systematics of the calculated work of separation correlates well with the noticeable variations of the charge-density values at the interface metal-C(N) bonds.

DOI: 10.1103/PhysRevB.69.125421

PACS number(s): 68.35.-p, 71.15.Nc, 73.20.At, 81.05.Je

I. INTRODUCTION

Joining ceramics with metals and other ceramics is of great interest in many different industrial applications. One of the most important joining techniques is brazing,¹ a process of joining materials by heating them in the presence of a filler (braze) metal above the melting point of the filler but below the melting points of the base materials. The same concept lies behind such an industrially important process as sintering of metal-ceramic composites, e.g., cemented carbides and cermets.^{2,3}

The first necessary condition for brazing is that the ceramics are wetted by the metallic braze. This condition is often difficult to meet with many important ceramics and conventional Cu- and Ag-based brazes. The important practical question is then how to improve wetting in those metal-ceramic systems. The traditional approach to solving this wetting problem is to add reactive elements, most frequently Ti, to the braze. This improves wetting for many relevant metal-ceramic combinations.

The effect of reactivity on wetting, in particular, the mechanism of Ti-induced wetting, has been given much attention in recent experimental studies⁴⁻⁸ and theoretical analyses.^{9,10} A common observation is that reactive wetting of oxide, carbide, or nitride ceramics by Ti-containing melts involves formation of TiO, TiC, or TiN layers, respectively, as reaction products at the interface. As a consequence, after the reaction the wetting is essentially controlled by a newly formed interface between TiO, TiC, or TiN and the Cu- or Ag-based melt. Further, it has been observed that the wettability between Cu-Ti alloys and many ceramic oxides is practically independent of even significant variations in the nature of those oxides.⁴

The importance of metal/Ti(O,C,N) interfaces in the Ti-promoted reactive wetting has motivated a number of experimental studies of wetting of titanium oxides, carbides, and nitrides by liquid Cu, Ag, Al, and other metals and alloys.^{4,11-16} Several sessile-drop wetting experiments with nonreactive metals, such as Cu and Ag, on stoichiometric

TiC and TiN^{11,13} show the contact angles to be high, $\geq 110^\circ$. From this one concludes that these metals do not wet stoichiometric TiC and TiN. At the same time, Refs. 12 and 14 demonstrate that stoichiometric TiC can be wetted by Cu.

So far answers from wetting experiments are different even for the basic question whether Cu or Ag wet or do not wet TiC. Yet, a few recent reports¹²⁻¹⁴ have in common the observation that the wetting is more sensitive to factors of chemical nature, such as changes in the local chemical composition at the interface,¹³ than to long-range interactions. Thus, in a search for effective ways to improve wetting, chemical factors in the interface adhesion are the potentially most important source of guiding principles.

Unfortunately, such chemical factors at the interface are very difficult to measure or control directly under the conditions of realistic wetting experiments. This makes it challenging to resolve any atomic scale processes at a buried boundary between an imperfect polycrystalline Ti(C,N) sample and a liquid metal. Moreover, the many different contributing factors mask their individual roles in the large scale picture that results.

In spite of the complexity of the observed wetting phenomena, we can still expect that many or at least some of the experimental wetting trends can be related to a few simple microscopic parameters, such as the strength of metal-Ti and metal-C(N) bonds across a metal/Ti(C,N) interface. Such connections could significantly help us understand the relative importance and role of different factors in the observed wetting behaviors. Building such simplified pictures is a key step towards the development of more quantitative and detailed microscopic models of metal-ceramic wetting, and towards the finding of new possibilities to improve wetting.

In a search for simple microscopic pictures of the wetting processes, first-principles computational experiments can provide valuable insights.¹⁷⁻²⁴ First-principles density-functional-theory (DFT) simulations typically give quite an accurate and reliable description of the energetics and electronic structure for the chemical bonding between different atoms in different chemical environments.

The present paper explores the correlations between the energetics of chemical bonds in a series of simulated Cu,Ag,Au/Ti(C,N) model interface systems and experimental wetting behaviors. A key question concerns how well the experimental adhesion energetics can be described in terms of the strength and relative number of metal-Ti and metal-C(N) bonds across the interface. This also gives an idea of to what extent the intrinsic metal/Ti(C,N) wettability is masked by various extrinsic effects. In particular, it is desirable to discriminate among the contradictory wetting experiment data, to judge which of the experiments are more likely to have been affected by some extrinsic effects, such as substrate surface contamination.

Another important question in this paper is to find factors that are responsible for the observed improved wettability of hypostoichiometric carbides and nitrides, TiC_x and TiN_x , $x < 1$, by Cu and Ag.^{11,13} This situation is an interesting example of how different factors interplay in the wetting behavior. On the one hand, the wettability can be improved by the presence of vacancies in the interface region. The latter affect the strength of the metal-Ti and metal-C(N) bonds across the interface. On the other hand, in the experimental report¹³ the better wettability is attributed to increased concentration of Ti in solution in the melt and to Ti segregation near the interface. To analyze those two possible mechanisms, a simple treatment of Ti(C,N) nonstoichiometry effects is included. Vacancies are introduced into the Ag/Ti(C,N)(001) system, and the limiting case of Ag/Ti interfaces with no C or N atoms is considered. To estimate the effect of the interface segregation of Ti, the systems Ti/Ti(C,N)(001) are considered. To evaluate the role of possible segregation of Al, a common additive used to improve wetting, we also study the Al/Ti(C,N)(001) model systems.

The paper is organized as follows. Sections II–V cover important methodological points of our study. The results of our computer simulations and theoretical analysis are presented and discussed in Secs. VI and VII. Section VIII summarizes our conclusions.

II. COMPUTATIONAL METHOD

Our electron-structure and total-energy calculations are based on the density-functional theory (Refs. 25–27) (DFT) with the Perdew-Wang 1991 version of the generalized gradient approximation²⁸ (GGA-PW91). We use the plane-wave pseudopotential method²⁹ implemented in the Vienna *ab initio* simulation package^{30–34} (VASP) with its standard set of Vanderbilt ultrasoft pseudopotentials.^{35,36}

The Kohn-Sham equations are solved with an iterative unconstrained band-by-band matrix-diagonalization scheme based on the residual minimization method,³⁴ updating the charge density via the Pulay mixing.³⁷ The plane-wave cutoff is taken to be 26 Ry (354 eV), which provides good absolute energy convergence of within 3 meV/atom for all elements studied. The Brillouin zone is sampled with Monkhorst-Pack³⁸ k -point grids with grid densities corresponding to at least $10 \times 10 \times 10$ k points in the primitive bulk cell. The specific grid dimensions will be given below. The Brillouin zone integration is done using the Methfessel-

TABLE I. Equilibrium lattice constants a_0 , bulk moduli B , and cohesive energies E_{coh} of Cu, Ag, Au, Al, Ti, TiC, and TiN from present plane-wave pseudopotential (PWPP) calculations.

Crystal	a_0 (Å)	B (Mbar)	E_{coh} (eV)
Cu(fcc)	3.644	1.39	3.51
Ag(fcc)	4.167	0.89	2.47
Au(fcc)	4.183	1.32	3.00
Al(fcc)	4.044	0.73	3.42
Ti(fcc)	4.096	1.05	5.19
TiC	4.343	2.47	7.32
TiN	4.258	2.77	6.85

Paxton smearing³⁹ of $\sigma = 0.15$ during structure optimizations and then applying the tetrahedron method with Blöchl corrections⁴⁰ to calculate the total energies and electronic structures. Structure relaxations are performed with a quasi-Newton algorithm and the analytical Hellman-Feynman forces. The structures are optimized until the total energies are converged to at least 10^{-3} eV.

To characterize the accuracy of the above computational method, Table I presents our calculated values of the lattice constant, bulk modulus, and cohesive energy for all the bulk materials of interest here, in particular, for Cu, Ag, Au, Ti, and Al in the fcc structure and for TiC and TiN in their NaCl structures. The bulk calculations are done with $10 \times 10 \times 10$ Monkhorst-Pack k -point grids. The lattice constants, bulk moduli, and the bulk total energies are obtained from fits of the total energies at different volumes by the Murnaghan equation of state.⁴¹ The cohesive energies are given with respect to the total energies of spin-polarized atomic ground states calculated in large-sided, 8–12 Å, cubic supercells.

Values in Table I are in good agreement with accurate all-electron results.^{42–48} Although some deviations from experimental values can be noticed, such as the tendency to underbinding for Ag and Au, they are almost exclusively due to the use of the GGA. The GGA is on average better than the local-density approximation (LDA) to account for experimental data, and it is significantly better for Ti, TiC, and TiN.

TABLE II. Calculated energetics for coherent Cu,Ag,Au(001)/Ti(C,N)(001) interfaces in Fig. 1. The results for the ideal work of separation W_{sep} and interface energy γ for relaxed structures are provided. The lattice mismatch values show the in-plane expansion of the metal slabs in the interface systems used. Labels (a)–(c) correspond to structures in Figs. 1(a)–1(c), respectively.

Interface	Lattice mismatch (%)	W_{sep} (J/m ²)			γ (J/m ²)		
		(a)	(b)	(c)	(a)	(b)	(c)
Cu/TiC	16.1	2.68	0.32	1.56	0.64	2.99	1.76
Ag/TiC	4.1	1.57	0.28	0.87	0.95	2.24	1.65
Au/TiC	3.7	1.86	0.37	1.06	0.76	2.25	1.56
Cu/TiN	14.4	1.93	0.50	0.88	1.01	2.44	2.07
Ag/TiN	2.1	0.87	0.43	0.59	1.30	1.74	1.58
Au/TiN	1.8	0.85	0.82	0.84	1.39	1.42	1.41

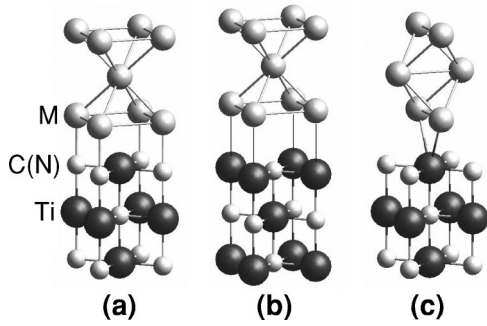


FIG. 1. The three $M(001)/Ti(C,N)(001)$ interface structures considered ($M=Cu, Ag, Au, Al, Ti$), with the M atom being over the C(N) (a), Ti (b), and bridge (c) sites. Half the elevation of the supercell is shown for each structure.

III. INTERFACE GEOMETRY

In theoretical modeling of interface systems one of the key points is an adequate choice of the interface geometry. Our interface geometry considerations employ the same general procedures as in our previous $Co/Ti(C,N)$ work.^{19,18} Due to periodic boundary conditions imposed by the plane-wave basis set, the interface systems are modeled by infinite periodic arrays of alternating metal and ceramic slabs. A simulation supercell contains one metal slab and one ceramic slab joined to give two equivalent interfaces per supercell without any vacuum layers.

As a first step, the slabs are taken as ideal truncations of the corresponding bulk crystals and put together in accordance with a chosen orientation relationship and relative translation and rotation of the contacting surfaces (translation and rotation states). The lattice parameters of the ceramics are kept like in unstrained bulk (Table I). The in-plane lattice constant of the metal phase is adjusted to give a commensurate structure with the ceramic slab. The metal out-of-plane lattice constant is optimized in bulk calculations to minimize the bulk strain introduced by the in-plane lattice distortion. The distance between the slabs is optimized to minimize the total energy of the system. The resulting system will be regarded as an unrelaxed interface. As a second step, all atomic positions within a few, typically two, outermost physical layers on each side of each slab are allowed to relax in all directions. The supercell size and the atomic positions in the

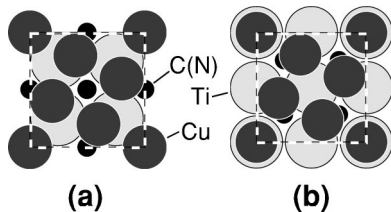


FIG. 2. The $Cu(001)/Ti(C,N)(001)$ interface structures with a relative rotation of the $Cu(001)$ and $Ti(C,N)(001)$ faces to reduce the interface lattice mismatch. The relative position of the interface Cu layer with respect to the surface $Ti(C,N)$ layer within one supercell is shown. Cases (a) and (b) correspond to the two high-symmetry translation states $5Cu/4Ti(C,N)$ -I and $5Cu/4Ti(C,N)$ -II, respectively.

middle layers are kept the same as in the unrelaxed system.

Most of our calculations are done for interfaces produced by the (001) surfaces of fcc metals and the (001) surface of TiC or TiN, that is, for the (001) \parallel (001) orientation relationship. Below we will use notations like $M/Ti(C,N)$, where M denotes the metal phase, $M = Cu, Ag, Au, Al, Ti$. As the original differences in lattice constants of Ag, Au, Al, Ti, and Ti(C,N) are within 7% (see Tables II and VII), simple coherent interface structures are used, like those in Fig. 1, without relative rotation of the contacting faces. In notations of Ref. 19 this is the $1M/1Ti(C,N)$ rotation state, with one primitive cell of $M(001)$ per 1 primitive cell of $Ti(C,N)(001)$. Only for $M = Cu$, which has a lattice mismatch of around 15% (Table II), we also use more complex structures in Fig. 2 with five Cu atoms per four C(N) atoms, i.e., a $5M/4Ti(C,N)$ rotation state. This decreases the lattice mismatch to 6.2% for $5Cu/4TiC$ and 4.3% for $5Cu/4TiN$ (Table III). For the $1M/1Ti(C,N)$ rotation state three different translation states are included [Figs. 1(a)–1(c)], which correspond to the metal M atom being over C(N), Ti, and bridge sites, respectively. For the $1M/1Ti(C,N)$ rotation state the same two high-symmetry translation states as in Ref. 19 are considered, denoted as $5Cu/4Ti(C,N)$ -I [Fig. 2(a)] and $5Cu/4Ti(C,N)$ -II [Fig. 2(b)].

To analyze the dependence on the interface orientation relationship, we choose a metal with a low metal/ $Ti(C,N)$ lattice mismatch ($\leq 4\%$), in particular, Ag, and consider $Ag(011)/Ti(C,N)(011)$ and $Ag(111)/Ti(C,N)(111)$ interfaces. For $Ag(011)/Ti(C,N)(011)$ there are four high-symmetry translation states displayed in Figs. 3(a)–3(d). For $Ag(111)/Ti(C,N)(111)$ we include two different terminations, $Ti(C,N)(111)$ -C(N) and $Ti(C,N)(111)$ -Ti with three high-symmetry translation states for each termination, as shown in Fig. 4.

For the $1M/1Ti(C,N)$ interface, which is the most important structure for our conclusions, only one middle layer in each slab was kept fixed (frozen) during atomic relaxation. The residual forces on the atoms of those frozen layers were zero, which is the result of the supercell symmetry. The largest residual forces in the frozen middle layers were in the $Ti(C,N)$ slabs of the $Ag(011)/Ti(C,N)(011)$ structures, reaching around 0.5 eV/\AA for some atoms. Yet, much of the interface energetics error from such residual forces should cancel out in the adhesion strength calculation, as those forces are similar in the interface systems and in the separated slabs.

TABLE III. Calculated values of the ideal work of separation W_{sep} and interface energy γ for the more complex $5Cu/4Ti(C,N)$ interfaces (Fig. 2) that have reduced mismatch strain. The results for both unrelaxed (Unrel) and relaxed (Rel) systems are presented.

Interface	Lattice mismatch (%)	Structure Fig	W_{sep} (J/m ²)		γ (J/m ²)	
			Unrel	Rel	Unrel	Rel
$5Cu/4TiC(001)$ -I	6.2	2(a)	1.40	1.42	1.95	1.47
$5Cu/4TiC(001)$ -II	6.2	2(b)	1.38	1.82	1.97	1.07
$5Cu/4TiN(001)$ -I	4.3	2(a)	1.24	0.82	1.90	1.65
$5Cu/4TiN(001)$ -II	4.3	2(b)	1.24	0.78	1.90	1.68

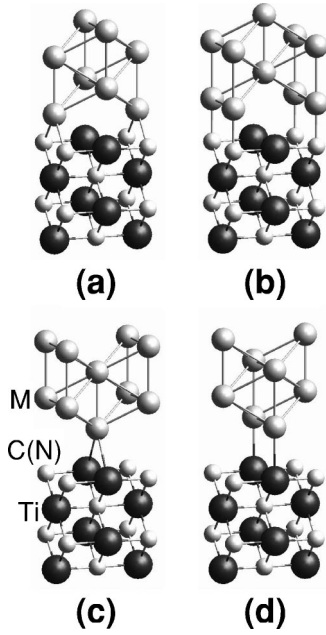


FIG. 3. The different M(011)/Ti(C,N)(011) interface structures studied ($M=Ag$). The atomic positions within half the elevation of the supercell are displayed. The difference between subfigures (a)–(d) is the relative translation of the metal M slab with respect to the Ti(C,N) one.

IV. WORK OF SEPARATION AND INTERFACE ENERGY DEFINITIONS

In experimental studies of interface energetics, e.g., sessile-drop wetting experiments, the most easily extractable energetics quantity is the *work of adhesion* (see, e.g., Ref. 17). This work is defined as the reversible free-energy change per unit area of interface for making free surfaces from interfaces. The free surfaces are then kept in equilibrium with the solid and gaseous components. From experimental values for the equilibrium wetting angle θ and the liquid surface energy (surface tension) σ one can evaluate the work of adhesion W_{ad} using the Young-Dupré equation¹⁷

$$W_{ad} = \sigma(1 + \cos \theta). \quad (1)$$

Unfortunately, at present a direct theoretical calculation of W_{ad} or θ from first principles is an unmanageable task. A related quantity, the *ideal work of separation* W_{sep} , can be calculated, however. The ideal work of separation is the reversible work that would be needed to cleave the interface into two free surfaces if the plastic and diffusional degrees of freedom were suppressed.¹⁷ It is a direct measure of the mechanical strength of the interface adhesion. In a repeated-slab interface geometry, W_{sep} can be calculated as (see, e.g., Ref. 49)

$$W_{sep} = (E_{sl1} + E_{sl2} - E_{int})/2A, \quad (2)$$

where E_{int} is the total energy of the supercell with the interface system, E_{sl1} and E_{sl2} are the total energies of the same supercell, when one of the slabs is kept and the other one is replaced by vacuum, and A is the interface area within one supercell. The factor 2 in the denominator accounts for the

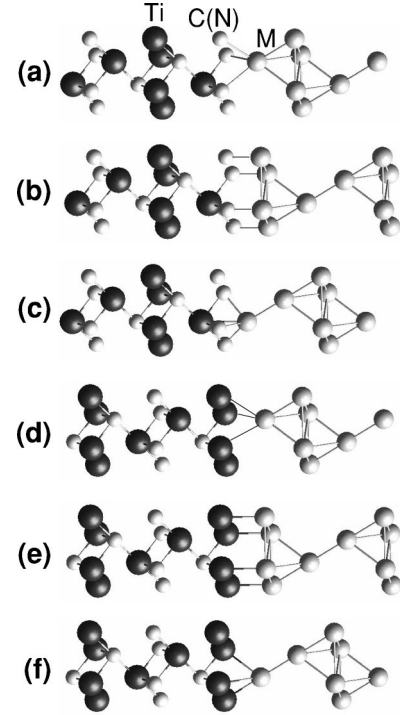


FIG. 4. Half the elevation of the supercell for the M(111)/Ti(C,N)(111) interface structures considered ($M=Ag$). Different high-symmetry translation states for the Ti(C,N)(111)-C(N) (a)–(c) and Ti(C,N)(111)-Ti (d)–(f) surface terminations are displayed.

fact that there are two (identical) interfaces per supercell. To calculate W_{sep} for the unrelaxed and relaxed interface structures we use the unrelaxed and relaxed values of $E_{sl1,2}$, respectively. As noted in Ref. 17, the behavior of W_{sep} can give only qualitative conclusions about the behavior of W_{ad} from Eq. (1).

For phases grown inside some medium, for instance, reaction products at the interface, an important quantity is the *interface energy*. For example, it determines the energetically preferred crystal faces, which in turn control the shape of the newly formed phase. The interface energy can be defined as the excess free energy associated with a unit area of interface. A simplified view of the interface energy is that it shows how much weaker the bonding is at the interface than the interlayer bonding in the corresponding bulk materials. For the model interface systems studied here, the interface energy is calculated as

$$\gamma = (E_{int} - E_{sl1}^{(b)} - E_{sl2}^{(b)})/2A, \quad (3)$$

where $E_{sl1}^{(b)}$ and $E_{sl2}^{(b)}$ are the bulk energies of the slabs, calculated for the slab size as given. To minimize numerical errors, the bulk energies are calculated with the supercells similar to the ones used for the interface calculations.

The ideal work of separation (2) and the interface energy (3) are related via the Dupré equation¹⁷

$$W_{sep} = \sigma_1 + \sigma_2 - \gamma, \quad (4)$$

where $\sigma_{1,2}$ are the surface energies of the separated slabs,

$$\sigma_{1,2} = (E_{s/1,2} - E_{s/1,2}^{(b)})/2A. \quad (5)$$

V. CONVERGENCE TESTS

The quality of our computed results for interface energetics is assessed through a series of extensive convergence tests. We choose one important interface structure, the one in Fig. 1(a), and consider variations of the ideal work of separation with changing plane-wave cutoff, k -point sampling, and number of layers in each slab. The tests cover all combinations of metals and ceramics of interest, $M/\text{Ti}(\text{C,N})(001)$, $M = \text{Cu, Ag, Au, Al, Ti}$. With the chosen plane-wave cutoff of 26 Ry, the work of separation is converged to within at least 0.03 J/m^2 for all the systems. Our convergence tests with respect to the k -point meshes and slab thicknesses show that with the chosen $10 \times 10 \times 2$ k -point sampling and five-layer thick slabs the convergence error is within about 0.1 J/m^2 . Note that since in such a sampling the two k points along the z axis are symmetry equivalent, only one irreducible k point along the z axis is actually used. For the $\text{Ag}/\text{Ti}(\text{C,N})(011)$ interfaces we take a $10 \times 8 \times 2$ k -point mesh and seven-layer slabs. The $\text{Ag}/\text{Ti}(\text{C,N})(111)$ interfaces are modeled with seven-layer metal and $7\text{C}(\text{N})+6\text{Ti}$ [Figs. 4(a)–4(c)] or $6\text{C}(\text{N})+7\text{Ti}$ [Figs. 4(d)–4(f)] ceramic slabs, with a $12 \times 12 \times 2$ k -point mesh. This is to provide accuracy at least similar to the $M/\text{Ti}(\text{C,N})(001)$ case.

VI. TRENDS IN INTERFACE ENERGETICS

A. Adhesion of Cu, Ag, and Au to $\text{Ti}(\text{C,N})(001)$

Our main results on the energetics of the $\text{Cu, Ag, Au}/\text{Ti}(\text{C,N})(001)$ interfaces are summarized in Tables II and III. For simple coherent structures in Fig. 1 only results for relaxed interfaces are included. The contribution of the relaxation effects to the interface energetics is around 0.1 J/m^2 for $\text{Cu, Ag, Au}/\text{TiC}$ and up to $0.2\text{--}0.3 \text{ J/m}^2$ for $\text{Cu, Ag, Au}/\text{TiN}$. The relaxation effects are stronger for the more complex structures in Fig. 2 (Table III), where there is some degree of interface incoherence.

Among the coherent interface structures, the structure with the metal atom over the C(N) site [Fig. 1(a)] is always energetically most favorable (Table II). This site preference is quite pronounced for all of the $\text{Cu, Ag, Au}/\text{Ti}(\text{C,N})$ systems, except Ag/TiN and Au/TiN . The value of the work of separation for the structure in Fig. 1(c), with the metal atom over the bridge site, is close to an average of the corresponding values for the metal over the C(N) and Ti sites [Figs. 1(a) and 1(b)]. The only noticeable deviation from this behavior is the case of Cu/TiN . For the preferred interface structures there is a clear trend that, for the same metal, adhesion to TiC is noticeably stronger than to TiN. In a series of Cu, Ag, and Au metals, for a given ceramic and given structure, the strongest adhesion is for Cu, and the weakest is for Ag. The only exception is the case of Ag/TiN and Au/TiN in their preferred structure [Fig. 1(a)], where bonding to Ag and Au is practically of the same strength.

At least for TiC, it is known that the (001) plane is a well-defined cleavage plane.⁵¹ This clean surface has significantly lower surface energy than, for instance, $\text{Ti}(\text{C,N})(011)$

TABLE IV. Calculated surface energy σ in units of J/m^2 for (001), (011), and (111) surfaces of TiC, TiN, and fcc Ti. Values for both unrelaxed (Unrel) and relaxed (Rel) structures are included. The present values for $\text{TiC}(001)$ and $\text{TiC}(011)$ surface energies are systematically by around 0.1 J/m^2 higher than those in Ref. 52, which is probably because Ref. 52 uses Ti pseudopotential with explicit $3p$ semicore states.

Surface	TiC		TiN		Ti	
	Unrel	Rel	Unrel	Rel	Unrel	Rel
(001)	1.88	1.73	1.68	1.38	1.83	1.71
(011)	4.05	3.78	3.16	2.83	2.06	2.00
(111)	5.91	5.63	4.98	3.62	1.96	1.89

or $\text{Ti}(\text{C,N})(111)$ surfaces (Table IV and Ref. 52). Hence, the $\text{Ti}(\text{C,N})(001)$ surface should be one of the main faces of $\text{Ti}(\text{C,N})$ powder grains. In experimental studies of wetting of $\text{Ti}(\text{C,N})$ by metals^{11–14} the ceramic substrate is typically made by sintering the $\text{Ti}(\text{C,N})$ powder. Thus, the $\text{Ti}(\text{C,N})$ substrate surface is likely to be built of $\text{Ti}(\text{C,N})(001)$ surfaces of the $\text{Ti}(\text{C,N})$ powder grains. That makes metal/ $\text{Ti}(\text{C,N})(001)$ interfaces a relevant case, when analyzing metal-on- $\text{Ti}(\text{C,N})$ wetting experiments.

The available reports on wetting experiments with liquid metals on $\text{Ti}(\text{C,N})$ ^{11–14} give a variety of results (Table V). According to Ramqvist,¹¹ Cu does not wet stoichiometric TiC, with a contact angle being 112° . Li¹² has demonstrated that wetting of TiC by nonreactive liquid metals, Cu, Ag, and Au, is improved significantly by reducing oxygen contamination of the substrate surface. For Cu on stoichiometric TiC, in the argon atmosphere and in the presence of a Ti getter furnace semitube, the reported wetting angle is 73° . Wetting angle was further reduced, to as low as 56° , by introducing a zirconium semitube in the system. However, in experiments of Xiao and Derby,¹³ even with very low oxygen pressure, the wetting angles for Cu and Ag on stoichiometric TiC and TiN are around 120° . A more recent experimental work of Froumin *et al.*¹⁴ concludes that the wetting of TiC by Cu is controlled by a partial dissolution of the TiC phase. When this dissolution process is inhibited by oxygen contamination, a nonwetting behavior occurs. If this oxygen effect is suppressed, e.g., by adding a small amount of Al in the Cu melt, the wettability is improved.

The data from wetting experiments relate to our theoretical results. In Tables II and III we compare the calculated values for the ideal work of separation with estimates of the interface adhesion work, W_{ad} (Table V). The latter values are based on Eq. (1) and the experimental values of the wetting angles.^{11–14} The necessary data for the surface tension σ are taken from Ref. 50 for Ag and Cu, and Ref. 53 for Au.

Although the values of the adhesion work W_{ad} vary from experiment to experiment (Table V), each of those values is covered by the corresponding region of calculated values of the ideal work of separation (Table II). That is, for a given combination of metal and ceramic, the experimental values of W_{ad} from Table V are typically between the minimal and maximal values of W_{sep} in Table II. This observation allows us, for pedagogical reasons, to represent W_{ad} as

TABLE V. Values of the adhesion work estimated from Eq. (1) and experimentally measured wetting angles θ at different temperatures T from available reports (source). The estimation uses values of the liquid metal surface tension σ at the specified temperatures extracted from the data of Ref. 50 for Ag and Cu, and from Ref. 53 for Au. Parameter α is defined by Eq. (6).

Interface	T ($^{\circ}\text{C}$)	θ ($^{\circ}$)	σ (J/m^2)	W_{ad} (J/m^2)	α	Source
Cu/TiC	1100	112	1.32	0.83	0.8	Ramqvist (Ref. 11)
	1100	73	1.32	1.71	0.4	Li (Ref. 12)
	1100	56	1.32	2.06	0.3	Li (Ref. 12)
	1150	126	1.30	0.54	0.9	Xiao and Derby (Ref. 13)
	1150	89	1.30	1.32	0.6	Froumin <i>et al.</i> (Ref. 14)
Ag/TiC	1100	78	0.89	1.08	0.4	Li (Ref. 12)
	1050	153	0.90	0.10	≈ 1	Xiao and Derby (Ref. 13)
Au/TiC	1100	105	1.14	0.85	0.7	Li (Ref. 12)
Cu/TiN	1150	110	1.30	0.86	0.8	Xiao and Derby (Ref. 13)
Ag/TiN	1050	143	0.90	0.18	≈ 1	Xiao and Derby (Ref. 13)

$$W_{ad} \approx (1 - \alpha)W_{sep}^{(a)} + \alpha W_{sep}^{(b)}, \quad 0 < \alpha < 1, \quad (6)$$

where $W_{sep}^{(a)}$ and $W_{sep}^{(b)}$ are the values of W_{sep} in columns (a) and (b) of Table II, respectively. The values of α , the weight factor, for each experimental value of W_{ad} are listed in Table V, numbers that we will return to.

In two cases of Table V values of W_{ad} are small, 0.10 J/m^2 for Ag/TiC and 0.18 J/m^2 for Ag/TiN, even smaller than $W_{sep}^{(b)}$. This is likely to reflect the higher sensitivity to the details and errors of the experiment and calculations for so small values of W_{ad} and W_{sep} . For example, it is known that in a system with poor wetting there is typically an increase of the wetting angle due to roughness of the substrate surface.⁴ In this situation it is sufficient that W_{ad} is of the same order of magnitude as $W_{sep}^{(b)}$, and also that $W_{sep}^{(a)} \gg W_{sep}^{(b)}$, to assume that α is close to unity.

Equation (6) allows a simple physical interpretation. The atomic structure of an interface between the liquid metal drop and the ceramic substrate is viewed as being a mixture of metal-over-C(N) [Fig. 1(a)] and metal-over-Ti [Fig. 1(b)] local atomic coordinations. The measured adhesion work is a weighted average of the work of adhesion/separation for the two elementary structures. The weight factor α shows what fraction of local atomic coordinations is represented by the metal-over-Ti configurations. We use this simplified picture to rationalize the correlations between the experimental observations and different sets of our theoretical results.

An example of a situation with a mixture of different atomic configurations is provided by the $5\text{Cu}/4\text{Ti}(\text{C},\text{N})$ interfaces (Fig. 2 and Table III). With an unrelaxed geometry, four out of five Cu atoms in the interface layer of the supercell (see Fig. 2) are about as close to the Ti sites as to the C(N) sites of the $\text{Ti}(\text{C},\text{N})(001)$ surface. In agreement with the above simple picture, the unrelaxed work of separation, W_{sep} , for those structures is close to an average of $W_{sep}^{(a)}$ and $W_{sep}^{(b)}$, i.e., $W_{sep} \approx 0.5W_{sep}^{(a)} + 0.5W_{sep}^{(b)}$. The change of W_{sep} during structure relaxation can be viewed as a shift in the balance between different local configurations.

In experimental systems the relative weights of the different atomic configurations are determined by many different

factors, such as the initial state of the substrate surface, local structural and compositional changes in the substrate due to its interaction with the melt, local correlations between the motion of different atoms of the liquid metal, and the relation between interatomic distances in the melt and in the substrate. In our analysis all these factors are accounted for by one parameter α . The value of this parameter indicates what atomic coordinations are likely to dominate, and, hence, what chemical interactions control the interface adhesion in a given metal-ceramic system.

An interesting systematic is observed in the experimental nonwetting behavior for Cu and Ag on stoichiometric TiC and TiN.¹³ The values of α (Table V) are all close to unity. This is due to the fact that the calculated values of the work of separation $W_{sep}^{(b)}$ (Table II) approach the small values of W_{ad} from experiment only for the metal-over-Ti configuration [Fig. 1(b)]. A somewhat similar situation is with Cu on TiC (Ref. 11) and Au on TiC.¹² One more important trend is the stronger adhesion to TiN than to TiC (Ref. 13) observed for a given metal (see Table V). In our calculated results, only the $W_{sep}^{(b)}$ values are consistent with that behavior. This indicates that a typical atomic coordination at the interface is likely to be with the metal atom over the Ti site. Thus, in this case the interface adhesion should be controlled by interatomic metal-Ti interactions across the interface.

In a situation of good wetting, as for Cu/TiC and Ag/TiC in the experiments of Ref. 12, parameter α becomes less than 0.5 (Table V). This indicates that there is a significant contribution of the metal-over-C(N) atomic coordinations [Fig. 1(a)] to the interface adhesion. That is, there is a sufficiently large number of the liquid metal atoms located at the C(N) sites of the substrate surface. On the boundary between wetting and nonwetting, represented by the results of Ref. 14, parameter α is slightly larger than 0.5. This corresponds to a relatively balanced mixture of the metal-over-Ti and metal-over-C(N) local atomic configurations at the interface.

From the above analysis we conclude that wetting or nonwetting behavior in the considered metal-ceramic systems can be connected to the relative role of metal-over-Ti and

metal-over-C(N) atomic coordinations at the interface under given experimental conditions.

B. Dependence on relative orientation

In an experimental study of the reactive wetting process of Ag-Cu-Ti on SiC (Ref. 6) the growth of the TiC nanoparticles, the reaction product, was observed to be accompanied by a change of particle shapes from round to polyhedral. One determining factor for the particle shape is the relation between interface energies of different metal/TiC interface orientations. To understand it, we analyze the orientational dependence of the interface energetics, for simplicity, that of Ag/Ti(C,N), with its relatively low lattice mismatch (Table II).

To get an insight into the orientational dependence of the Ag/Ti(C,N) interface energetics, values of the ideal work of separation and interface energy are calculated for Ag(001)/Ti(C,N)(001), Ag(011)/Ti(C,N)(011), and Ag(111)/Ti(C,N)(111) (Figs. 5 and 6). In addition, the situations of this metal-ceramic interface, Ag/Ti(C,N), and of a metal-metal one, Ag/Ti, are compared.

There is an ambiguity in the definition of the Ag/Ti(C,N)(111) interface energy or Ti(C,N)(111) surface energy. This is due to the presence of two different terminations of the Ti(C,N)(111) surface, Ti(C,N)(111)-Ti and Ti(C,N)(111)-C(N). When a bulk Ti(C,N) is cleaved to produce two Ti(C,N)(111) surfaces or Ag/Ti(C,N)(111), the two different terminations are created simultaneously. Such a

cleavage experiment does not allow an unambiguous split of the total cleavage energy into the surface energies of the two terminations. For simplicity, without any implications for our wetting analysis, here we consider only the average of the surface energies of the Ti(C,N)(111)-Ti and Ti(C,N)(111)-C(N) terminations. In other words, we assume that the two different terminations have the same surface energies (Table IV). Then we calculate the interface energy, using Eqs. (4) and (5). Typically the TiC(111) surface occurs when a TiC film is grown. In such growth experiments a free TiC(001) surface in vacuum is always Ti-terminated,⁵⁴ as discussed in Ref. 55.

The results for the orientational dependence of the ideal work of separation W_{sep} and interface energy γ are presented in Figs. 5 and 6. As illustrated by the above discussion of the Cu,Ag,Au(001)/Ti(C,N)(001) adhesion, our understanding of the experimental wetting behaviors can benefit from a consideration of different atomic coordinations, not only the energetically most favorable one. Due to this, Figs. 5 and 6 include the results for all the interface structures in Figs. 1, 3, and 4.

For the energetically favorable structures of Ag/Ti(C,N) interfaces [Figs. 1(a), 3(a), 4(c), and 4(f)], there is a noticeable increase both of W_{sep} and γ in the series of (001)|| (001), (011)|| (011), and (111)|| (111) (Figs. 5 and 6). Such a behavior of γ implies that, at least for structurally well-ordered Ag/Ti(C,N) interfaces, the (001)|| (001) orientation relationship gives the lowest interface energy. It is interesting to note that for interfaces between fcc metal and fcc oxides the (001)|| (001) orientation relationship (“cube-on-cube”) is the one that is most frequently observed in experiments.⁵⁶

In a wetting experiment with a liquid metal on a Ti(C,N) substrate different atomic configurations can occur, due to a

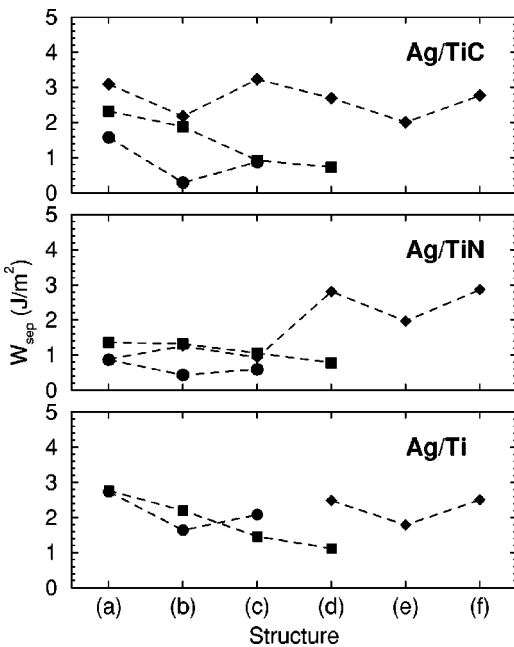


FIG. 5. Structure dependence of the ideal work of separation W_{sep} for Ag/TiC, Ag/TiN, and Ag/Ti interfaces. Circles, squares, and diamonds represent (001)|| (001), (011)|| (011), and (111)|| (111) interface orientation relationships, respectively. Labels (a)–(f) refer to the labels of the subfigures of Figs. 1, 3, and 4. Those labels distinguish different interface translation states for a given orientation relationship. The plotted values are for relaxed structures.

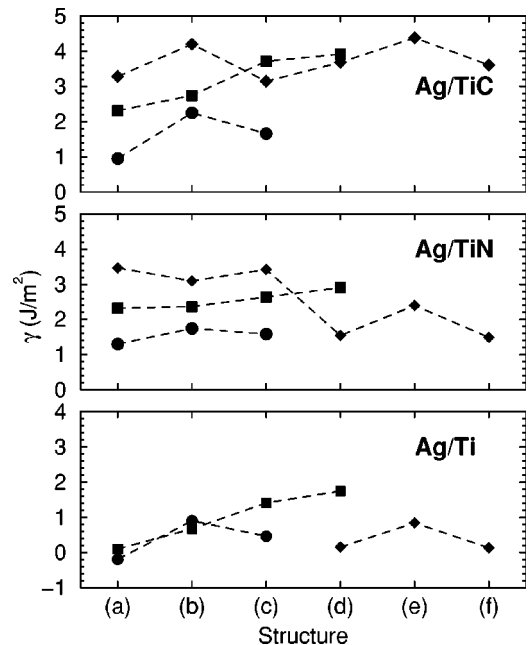


FIG. 6. Structure dependence of the interface energy γ for the Ag/TiC, Ag/TiN, and Ag/Ti systems. Structures and notations are the same as in Fig. 5.

disordered interface structure. In Fig. 6 there is some overlap between the regions of γ values covered by different structures of a given orientation relationship. This means that, under some experimental conditions, there is a possibility for a coexistence of different faces of the Ti(C,N) particles in a Ag melt. A change in the experimental conditions can change the relation between the interface energies of different orientations, modifying the Ti(C,N) particle shapes.

As can be understood with the help of relation (4), a simultaneous growth of W_{sep} and γ from Ag(001)/Ti(C,N)(001) to Ag(011)/Ti(C,N)(011) and Ag(111)/Ti(C,N)(111) is connected to the larger change of the Ti(C,N) surface energy from one orientation relationship to another than for the work of separation.

For the metal-metal Ag/Ti interface the relative changes of the work of separation with the orientation are quite small (Fig. 5). The Ag/Ti interface energy is much smaller than any of the Cu,Ag,Au/Ti(C,N) interface energy values (Tables II, III, and Fig. 6). The increase of the interface energy by around 0.3 J/m² from Ag(001)/Ti(001) to Ag(011)/Ti(011) and Ag(111)/Ti(111) gives a large relative change and alternates the interface energy sign.

The key difference between different structures in Figs. 1, 3, and 4 lies in the number of bonds between Ag and Ti and C(N) atoms, respectively, at the interface. When counting the number of Ag-Ti and Ag-C(N) bonds it is important that there is a drastic difference in the characteristic lengths of those bonds. Throughout all the interface structures studied, the relaxed Ag-Ti bonds are never shorter than about 2.8 Å, while typical Ag-C(N) bond lengths are around 2.0 Å. As a consequence, when the interface Ag atom is placed over the Ti site, such as in Figs. 1(b), 3(d), and 4(e), the Ag and C(N) atoms are too far apart for any noticeable Ag-C(N) bonding. For the case of Ag atoms near the C(N) sites, like in Figs. 1(a), 3(a), and 3(b), the Ag atoms still participate in a number of Ag-Ti bonds. This bond-counting picture agrees well with the structural dependence of interface adhesion energetics for Ag on Ti(C,N)(001), Ti(C,N)(001), and Ti-terminated TiC(111). In particular, Fig. 5 shows that the energetically most favorable structures for those interfaces [Figs. 1(a), 3(a), and 4(f)] are the ones that have maximal total number of Ag-C(N) and Ag-Ti bonds per Ag atom.

When connecting the orientation dependence of W_{sep} with the number and strength of the interface Ag-C(N) and Ag-Ti bonds, one should also consider the number of Ag atoms per unit area of the interface, or, equivalently, the interface area per one Ag atom. The values of the interface area per Ag atom are approximately $0.5a^2$, $0.707a^2$, and $0.433a^2$ for (001)∥(001), (011)∥(011), and (111)∥(111) orientation relationships of Ag/Ti(C,N), respectively. Here a is the lattice parameter of TiC or TiN.

The difference in the interface area per atom is important, e.g., when comparing the Ag/Ti(C,N)(001) and Ag/Ti(C,N)(011) systems. The work of separation per Ag atom is a little more than twice as large for the Ag/Ti(C,N)(011) structure in Fig. 3(a) than for the Ag/Ti(C,N)(001) structure in Fig. 1(a), which correlates with the fact that there are twice as many Ag-C(N) bonds at that Ag/Ti(C,N)(011) inter-

face than at Ag/Ti(C,N)(001). However, this relative difference is less noticeable in the W_{sep} values per unit area (Fig. 5).

In the orientational dependence of the interface adhesion, another important factor is the strength of the Ag-Ti bonding, which is controlled by the number of the nearest C(N) neighbors around the interface Ti atoms. This number equals 5, 4, and 3 at the Ti(C,N)(001), Ti(C,N)(011), and Ti-terminated Ti(C,N)(111) surfaces, respectively, to be compared with six in bulk TiC(N). When there is a large number of C(N) neighbors around the interface Ti atom, like for Ti(C,N)(001) (Fig. 1), the Ag-Ti bonding at the Ag/Ti(C,N) interfaces is substantially weaker than at the Ag/Ti interface, as rationalized in Sec. VII A. This is most clearly seen from the calculated values of W_{sep} (Fig. 5) for the metal-over-Ti structure [Fig. 1(b)], which are much smaller for Ag/Ti(C,N) than for Ag/Ti. In the metal-over-C(N) structure of Ag/Ti(C,N) [Fig. 1(a)] the weakening of the four Ag-Ti bonds is not compensated by the creation of one Ag-C(N) bond, and W_{sep} is smaller than for the similar metal-over-interstitial structure of Ag/Ti. A case with only three C(N) neighbors around the interface Ti atom is represented by the Ti-terminated Ti(C,N)(111) surface [Figs. 4(d)–4(f)]. Figure 5 demonstrates that W_{sep} for Ag on Ti(C,N)(111)-Ti behaves very similar to the case of Ag/Ti(111). Thus, the fewer C(N) neighbors per Ti atom, the stronger the Ag-Ti bonding.

C. Contribution of vacancies

As reported in experimental studies,^{11,13} wettability of TiC or TiN by Cu or Ag is quite sensitive to the Ti(C,N) stoichiometry. TiC and TiN can exist in a broad range of hypostoichiometric compositions, TiC_x and TiN_x, $x \leq 1$, retaining the fcc structure of the Ti sublattice. A decrease in the C(N) content introduces vacancies in the C(N) sites of Ti(C,N). The wettability of TiC_x by Cu or Ag and TiN_x by Cu improves with decreasing x , showing a nonwetting to wetting transition around $x = 0.5$ – 0.8 .^{11,13}

In an *ab initio* study⁵⁷ of a metal-oxide Ag/Mg(001) interface, vacancies and other charged effects are shown to contribute significantly to the interface adhesion. This conclusion is not directly transferable to metal-carbide or metal-nitride interfaces, as the nature of the interface bonding is essentially different.^{18,19} For an Fe/VN interface with vacancies, first-principles calculations⁵⁸ have shown that introduction of a bulk concentration of N vacancies leads to a considerable increase of the interface energy γ . However, vacancies also change the ceramic bulk energy in Eq. (3) and surface energy in Eq. (4). Thus, the increase of γ does not carry any information about the change of the interface bonding strength or W_{sep} , which is relevant for wetting.

To get an insight into the effect of vacancies on metal/Ti(C,N) adhesion, calculations of W_{sep} are performed for Ag(001)/Ti(C,N)(001) interfaces with vacancies. The interface structures with the Ag atoms over the C(N) [Fig. 1(a)] and Ti [Fig. 1(b)] sites are simulated in supercells of 4×4 lateral size, with five-layer thick Ag and seven-layer thick Ti(C,N) slabs. One C(N) vacancy is introduced on each side of the Ti(C,N) slab with the vacancy position varied from the

TABLE VI. Ideal work of separation W_{sep} in units of J/m^2 for coherent Ag(001)/Ti(C,N)(001) interfaces with C(N) vacancies in the 1st, 2nd, 3rd, and 4th layers from the interface, compared to the no-vacancy (none) case. Columns (a) and (b) correspond to structures with the Ag atoms over the C(N) [Fig. 1(a)] and Ti [Fig. 1(b)] sites. All values are for relaxed structures.

Vacancy position	Ag/TiC		Ag/TiN	
	(a)	(b)	(a)	(b)
First (interface) layer	1.75	0.49	1.23	0.55
Second layer	1.58	0.38	1.01	0.55
Third layer	1.52	0.26	0.86	0.42
Fourth layer	1.55	0.28	0.87	0.41
None	1.59	0.29	0.87	0.41

interface layer to the second and third layer. A situation with one vacancy in the middle (fourth) layer of the Ti(C,N) is also considered. The positions of all atoms in the supercell are allowed to relax, except the atoms of the middle layer of the Ag slab.

The resulting values of W_{sep} (Table VI) show that mainly vacancies of the first two Ti(C,N)(001) surface layers have a noticeable effect on the Ag/Ti(C,N) interface adhesion. In the Ag/TiC case there are also some oscillations of W_{sep} with vacancy position in the third and fourth layers from the interface. The addition of vacancies tends to increase W_{sep} , which is consistent with that W_{sep} for Ag/Ti is larger than for Ag/Ti(C,N) (Fig. 5), and with the experimental fact of better wettability of hypostoichiometric Ti(C,N).

A Ag/Ti(C,N) system with vacancies can be considered as an intermediate step between a no-vacancy Ag/Ti(C,N) case and a metal-metal Ag/Ti interface. We can make a simple linear extrapolation of the change of W_{sep} with addition of vacancies to the case of Ag/Ti, W_{sep}^{met} , as,

$$W_{sep}^{met} \approx W_{sep}^{(0)} + 4(\Delta W_{sep}^{(1)} + \Delta W_{sep}^{(2)}), \quad (7)$$

where $W_{sep}^{(0)}$ is W_{sep} for Ag/Ti(C,N) without vacancies, and $\Delta W_{sep}^{(1,2)}$ are the changes in W_{sep} with introducing a 1/4 monolayer of vacancies in the first and second layers from the interface, respectively. With the data in Table VI, Eq. (7) gives values of 1.45 and 1.53 J/m^2 for the Ag-over-Ti structures of Ag/TiC and Ag/TiN, respectively. This is quite close to the value of 1.64 J/m^2 for the corresponding Ag/Ti structure. For the Ag-over-C(N) structures, the W_{sep}^{met} estimate is 2.19 and 2.87 J/m^2 for Ag/TiC and Ag/TiN cases, respectively. The value for the Ag/TiN case compares quite well with the W_{sep} value of 2.73 J/m^2 for Ag/Ti. An extrapolation from the Ag/TiC case shows a more noticeable deviation from the Ag/Ti situation. An overall conclusion from this analysis is that the magnitude of the vacancy contribution to W_{sep} is quite consistent with the W_{sep} difference between the Ag/Ti(C,N) and Ag/Ti cases.

D. Ti/Ti(C,N) and Al/Ti(C,N)

In wetting of ceramics by liquid metals, an important issue concerns the roles of different metallic elements present

TABLE VII. Calculated values of the work of separation W_{sep} and interface energy γ for coherent Ti(001)/Ti(C,N)(001) and Al(001)/Ti(C,N)(001) interfaces (Fig. 1). Labels (a)–(c) correspond to Figs. 1(a)–1(c), respectively. The values given are for relaxed geometries.

Interface	Lattice mismatch (%)	W_{sep} (J/m^2)			γ (J/m^2)		
		(a)	(b)	(c)	(a)	(b)	(c)
Ti/TiC	5.7	3.81	0.70	2.57	-0.38	2.73	0.85
Ti/TiN	3.8	3.56	0.43	1.66	-0.48	2.65	1.42
Al/TiC	6.9	2.56	0.51	1.63	0.21	2.26	1.14
Al/TiN	5.0	1.47	0.76	0.80	0.94	1.65	1.61

in the melt. Those elements can be added to the melt directly, or they can be a result of substrate dissolution during the wetting process. Formation of a reaction product at the interface is not the only possible mechanism of how metal additive can affect wetting. Another important effect is the segregation of those additional elements near the interface. For wetting by Cu and Ag, two commonly used additives are Ti and Al. In the case of Ti, even after the formation of the TiC or TiN reaction product at the interface, Ti can still be present in the melt, and its segregation at the interface can further affect wetting.

Interface segregation of Ti in Cu,Ag/Ti(C,N) systems is analyzed in wetting experiments,¹³ where electron microprobe scans of the liquid metal drops are done. Due to dissolution of Ti(C,N) into Cu or Ag melt, Ti is present in the metal drop even in the case of originally pure Cu or Ag drops. There is even higher concentration of dissolved Ti in the case of Cu-20%Ti/TiN.¹³ The microprobe scans clearly show that the Ti concentration rapidly increases towards the interface. Unfortunately, the spatial resolution of the scans is in the micrometer range, not allowing a determination of the Ti concentration in the first few metal layers at the interface. Yet, an upper limit on the effect of dissolved Ti on the interface adhesion can be estimated by considering a situation where Ti concentration approaches 100 at. % within a few near-interface atomic layers. We simulate this situation by fcc Ti(001)/TiC(001) and Ti(001)/TiN(001) model interface systems.

The concentration of Ti dissolved in the melt can be much larger for hypostoichiometric Ti(C,N) substrates than for stoichiometric ones.¹³ Thus, the issue of Ti segregation can be an important factor for the metal/Ti(C,N) wetting dependence on Ti(C,N) hypostoichiometry.

The effect of Al additions on wetting of TiC by liquid Cu has been addressed in experimental study.¹³ It is concluded that an Al-induced improvement of wetting is mainly due to an enhanced transfer of Ti into the Al-containing melt in the process of the TiC substrate dissolution. The Al segregation at Cu,Ag/Ti(C,N) interface has not been measured. To get an insight into a possible contribution of those effects, here we consider Al(001)/TiC(001) and Al(001)/TiN(001) systems.

In the calculated energetics of Ti,Al(001)/Ti(C,N)(001) (Table VII) the most drastic difference from the Cu,Ag,Au/Ti(C,N)(001) cases (Table II) is observed for the Ti/Ti(C,N) interface systems with metal atoms over the C(N)-sites [Fig.

1(a)]. The W_{sep} values are here noticeably larger, and the γ values are lower, than for any of the Cu,Ag,Au/Ti(C,N)(001) or Ag/Ti(001) systems. This shows a possibility that the interface segregation of Ti can have a noticeable effect on the interface adhesion in a metal/Ti(C,N)(001) system.

The values of W_{sep} and γ for the Al(001)/Ti(C,N)(001) interfaces are in about the same range as for Cu,Ag,Au/Ti(C,N)(001). The behavior of W_{sep} is somewhat similar to the Cu/Ti(C,N)(001) case. Thus, effects of Al segregation should not be of much significance for metal/Ti(C,N)(001) adhesion.

VII. NATURE OF BONDING

The key distinction of noble metals, such as Cu, Ag, and Au, from free-electron and transition metals is in that they have filled valence d shells. Hence, they are less chemically active than transition metals with partially filled d shells. This difference in the chemical activity correlates well with the experimentally measured wetting properties. As noted in, e.g., Ref. 11, transition metals wet metallic carbides much better than noble metals. This conclusion is also in line with theoretical results. In particular, the calculated values for the work of separation for Cu,Ag,Au/Ti(C,N)(001) (Tables II and III) are typically lower than for similar structures of Co/Ti(C,N) in Refs. 18 and 19. This difference in W_{sep} is very pronounced for structures with the metal atoms over the C(N) sites [Fig. 1(a)], for which W_{sep} for Co/Ti(C,N) is as large as 3.7–4.2 J/m².

At Co/Ti(C,N)(001), Co/WC(001), and TiC(100)/Fe(110) interfaces studied in Refs. 18–21, 52 the bonding is dominated by a particular kind of σ - pd covalent bonds between Co and C(N) atoms. The strength of the interface Co-C(N) bonds correlates with a very pronounced charge-density accumulation along those bonds. Here we analyze how those electronic structure features are modified when going from Co/Ti(C,N)(001) to Cu,Ag,Au/Ti(C,N)(001). For simplicity, we consider only interfaces with metal-over-C(N) structure [Fig. 1(a)].

Figures 7 and 8 show the distribution of the valence electron density at the Cu,Ag,Au/TiC(001) and Cu,Ag,Au/TiN(001) interfaces, respectively. One can clearly distinguish metal-C(N) bonds with a charge-density pattern similar to that at Co/Ti(C,N)(001) and Co/WC(001) in Refs. 18–21. The same density pattern is also seen at Ti/TiC(001) in Fig. 9(a). This type of density distribution is associated with p - d hybridization between transition metal d orbitals and C(N) p orbitals. This density pattern is not observed at, e.g., Al/TiC(001) in Fig. 9(b), where there are metal-C(N) bonds with a free-electron metal.

Like for Co/TiC(001), the charge density along the interface metal-C(N) bonds at Cu,Ag,Au/TiC(001) and Cu/TiN(001) is higher than along the bulk Ti-C(N) bonds. The charge-density values at the interface metal-C(N) bonds show noticeable variations from system to system. Those variations correlate well with the systematics of W_{sep} in Table II, in particular, with the differences between the Cu, Ag, and Au cases, as well as between the metal/TiC and metal/TiN systems. The highest charge density is at the Cu-C

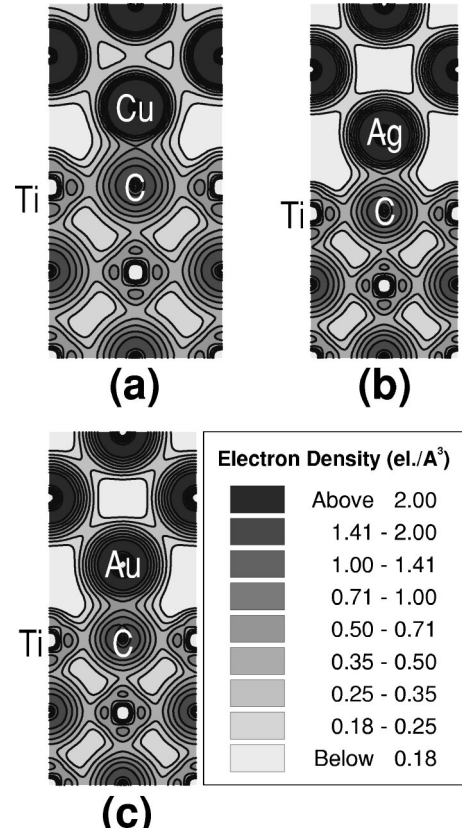


FIG. 7. Valence electron density for Cu(001)/TiC(001) (a), Ag(001)/TiC(001) (b), and Au(001)/TiC(001) (c) interfaces in the metal-over-C structure in Fig. 1(a), including atomic structure relaxation. The (010) cuts are shown. The consecutive contours change by a factor of $\sqrt{2}$ and the color bars are in units of electrons/Å³.

bonds at Cu/TiC(001), and the lowest is at the Ag/TiN(001).

Figures 10 and 11 present electronic local density of states (LDOS) at Cu,Ag,Au/TiC(001) and Cu,Ag,Au/TiN(001) interfaces, respectively. The LDOS is projected onto atomic orbitals of the interface atoms. A comparison with the LDOS of the same atoms in bulk materials (Fig. 12) shows that there is a noticeable hybridization between Cu, Ag or Au d orbitals and C(N) p orbitals. This is particularly clear for Ag/TiC [Fig. 10(b)], where there is a pronounced Ag- d LDOS peak in the same area as the C- p peak. This Ag- d peak occupies the energy region between about -3 and 0 eV, in which there is no significant d -band LDOS in bulk Ag [Fig. 12(a)]. A related situation is at the Cu/TiN interface [Fig. 11(a)], where hybridization with the N- p states noticeably modifies the bottom part of the Cu d band. At Cu/TiC and Au/TiC [Figs. 10(a) and 10(c)] the C-Cu,Au p - d hybridization is reflected in that the C- p LDOS become more uniformly distributed over the energy regions of the Cu or Au d bands. Thus, the behaviors of the electron density and projected LDOS show that the nature of the metal-C(N) bonding across Cu,Ag,Au/Ti(C,N)(001) interfaces is similar to that at Co/Ti(C,N)(001), Co/WC(001), or TiC(100)/Fe(110) in Refs. 18–21 and 52.

The difference in the strengths of the interface metal-C(N) bonds between metal/TiC and metal/TiN interfaces can be

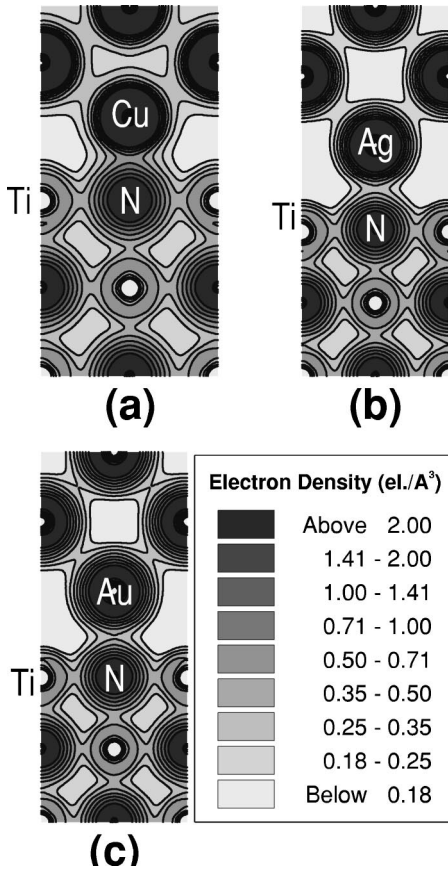


FIG. 8. Valence electron density for Cu(001)/TiN(001) (a), Ag(001)/TiN(001) (b), and Au(001)/TiN(001) (c) interfaces with the structure in Fig. 1(a), with structure relaxation. The (010) cuts are shown. The consecutive contours differ by a factor of $\sqrt{2}$ and the color bars are in units of electrons/ \AA^3 .

given a simple electron-structure explanation. When moving from bulk TiC to TiN, the extra electron of N goes to the Ti-C(N) antibonding orbitals, which are mainly located around the Ti atom (see Fig. 12). The N- p electrons in the Ti-C(N) bonding states become more tightly bound to the N nucleus, as the N nucleus has a higher positive charge than the C nucleus. As a consequence, the more tightly bound electrons of N in TiN create weaker p - d bonds across the interface than the C- p electrons in TiC. This effect should be of more significance than the relative shift of the C(N)- $2p$ in energy with respect to the metal d band, pointed out in Ref. 19 to explain the difference between Co/TiC(001) and Co/TiN(001). For example, at Ag/TiN(001) [Fig. 11(b)] the N- p LDOS has a larger overlap with the energy region of the Ag d band than the C- p LDOS at Ag/TiN(001) [Fig. 10(b)], while the bonding is stronger at Ag/TiC(001) than at Ag/TiN(001).

The situation of Ag can be distinguished from that of Cu and Au by that the valence charge density tends to be less spread out around the Ag atoms than around Cu or Au. This is seen in the metal bulk layers in Figs. 7 and 8). In addition, the Ag d band lies deeper in energy than the d bands of Cu and Au [Fig. 12(a)]. In particular, in Fig. 12(a) there is only negligible Ag- d DOS down to -3 eV from the Fermi level,

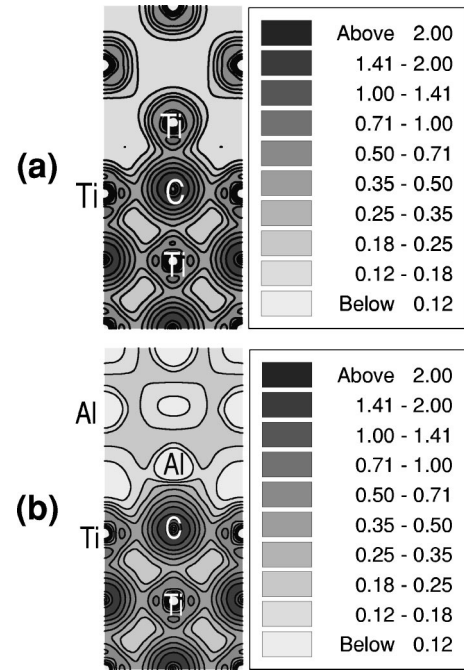


FIG. 9. The (010) cut of the valence electron density for Ti(001)/TiC(001) (a) and Al(001)/TiC(001) (b) with the structure in Fig. 1(a), with structure relaxation. The consecutive contours differ by a factor of $\sqrt{2}$ and the color bar is in units of electrons/ \AA^3 .

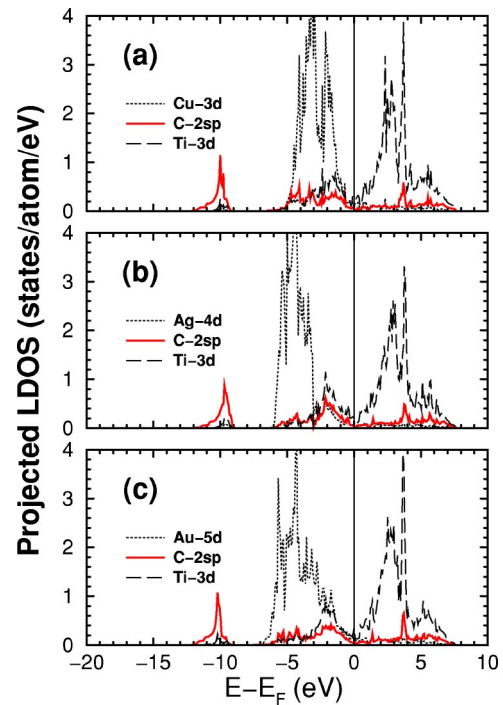


FIG. 10. The electronic local density of states (LDOS) at Cu(001)/TiC(001) (a), Ag(001)/TiC(001) (b), and Au(001)/TiC(001) (c) interfaces in the metal-over-C structure in Fig. 1, with structure relaxation. The main components of the LDOS projected onto atomic orbitals of the interface atoms are plotted.

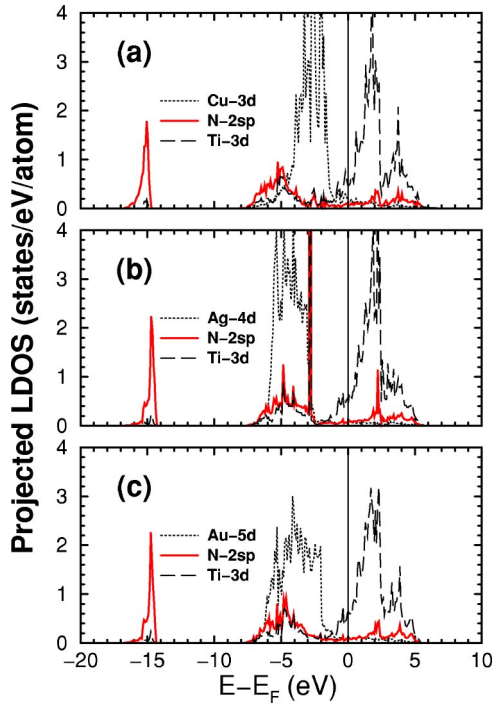


FIG. 11. The electronic LDOS projected onto atomic orbitals of the interface atoms at Cu(001)/TiN(001) (a), Ag(001)/TiN(001) (b), and Au(001)/TiN(001) (c) interfaces with structure in Fig. 1, including structure relaxation.

while there is significant Cu- d and Au- d DOS already -1.5 eV below the Fermi level. Those features indicate that the d -band states in Ag are more tightly bound than in Cu and Au. This explains why the interface metal-C(N) p - d bonding to Ti(C,N)(001) is weaker for Ag than for Cu or Au.

Figure 13 presents the distribution of the electron density along the Ag-C(N) bonds for the energetically preferred structures of Ag(001)/Ti(C,N)Ag(001) [Fig. 1(a)], Ag(001)/Ti(C,N)Ag(001) [Fig. 3(a)], and Ag(001)/Ti(C,N)Ag(001) [Fig. 4(c)]. For Ag/TiC, the density curves for the three different orientation relationships are practically identical. For Ag/TiN, only the (111) \parallel (111) case is somewhat different from (001) \parallel (001) and (011) \parallel (011). The overall conclusion from Fig. 13 is that variation of the interface orientation should not introduce any qualitative changes in the nature of the interface metal-C(N) bonds. Using a similar procedure, the same conclusion is drawn about the orientation dependence of the interface Ag-Ti bonds.

Figures 14(a) and 14(b) show the valence electron density around C(N) vacancies at the Ag/Ti(C,N)(001) interfaces. In the vacancy region the electron density distribution at Ag/Ti(C,N)(001) becomes closer to that at Ag/Ti(001) [Fig. 14(c)]. The projected LDOS for Ag/Ti(C,N)(001) with C(N) vacancies (Fig. 15) shows a slight vacancy-induced modification of the Ag- d and Ti- d components towards the situation of Ag/Ti(001) interface [Fig. 15(c)]. Thus, like the trends in the interface energetics, the electronic structure behaviors are consistent with that the Ag/Ti(C,N)(001) interfaces with vacancies can be viewed as an intermediate situation between stoichiometric Ag/Ti(C,N)(001) and metal-metal Ag/Ti(001) systems.

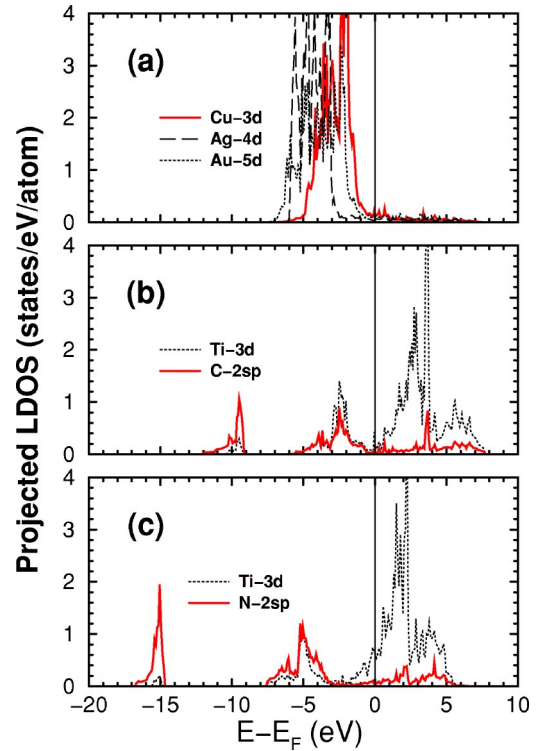


FIG. 12. The electronic LDOS projected onto atomic orbitals in bulk Cu, Ag, and Au (a), as well as in bulk TiC (b) and TiN (c).

A. Qualitative analysis of the trends in the metal-Ti bonding

The discussion in the previous sections demonstrates that an important role in metal/Ti(C,N) wetting behaviors should be played by the metal-Ti bonds. The most pronounced effect is the dependence of the metal-Ti bonding strength on the number of C or N neighbors around each interface Ti atom. This is the key to understanding of the C,N-vacancy contribution and orientation dependence for Ag/Ti(C,N) bonding. It should also explain why Ag-Ti bonding at Ag/TiC inter-

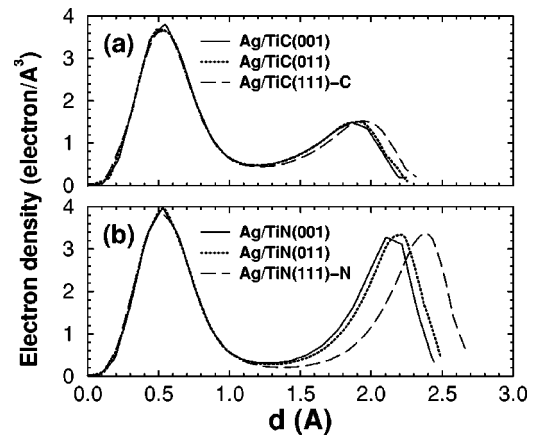


FIG. 13. Valence electron density along the interface Ag-C(N) bonds at Ag/TiC (a) and Ag/TiN (b), for Ag(001)/Ti(C,N)(001) (solid), Ag(011)/Ti(C,N)(011) (dotted line) and Ag(111)/Ti(C,N)(111) (long-dashed line) interfaces with structures in Figs. 1(a), 3(a), and 4(c), respectively. The structures are relaxed. The distance d is counted from the Ag atom.

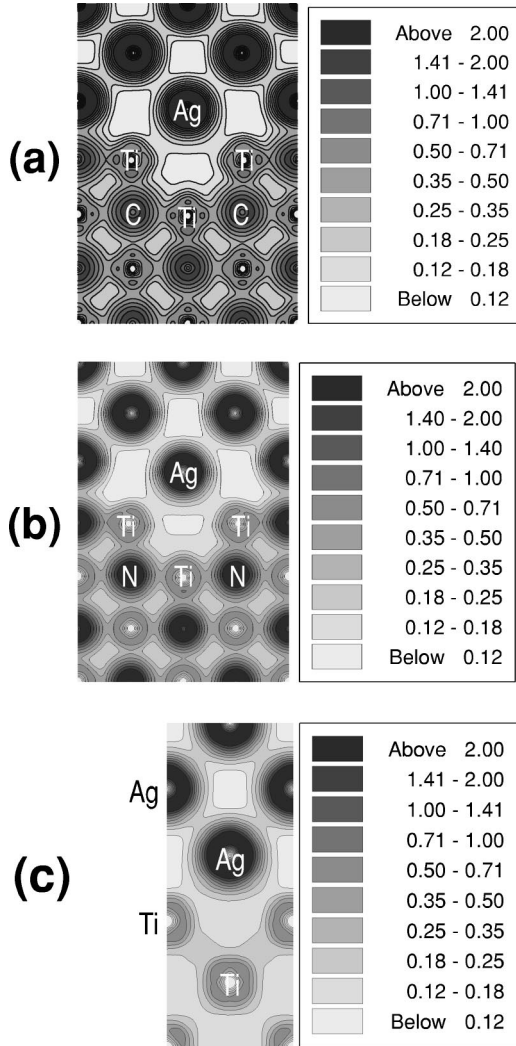


FIG. 14. Valence electron density at the Ag/TiC(001) (a) and Ag/TiN(001) (b) interfaces in the metal-over-C(N) structure [Fig. 1(a)] with a C(N) vacancy in the interface layer, in comparison with that at the metal-metal Ag(001)/Ti(001) interface (c). The (010) cuts are shown. The consecutive contours differ by a factor of $\sqrt{2}$ and the color bars are in units of electrons/ \AA^3 . The structures are relaxed.

face is weaker than at Ag/TiN one and why it is stronger at a metal-metal Ag/Ti interface than at Ag/Ti(C,N).

These behaviors can be given a simple electronic structure interpretation based on a qualitative analysis of the LDOS of free slabs of Ag, Ti, TiC, and TiN (Fig. 16) within an approximate perturbation-theory picture of the orbital interactions.^{59–61}

The analysis naturally starts from two noninteracting systems, like atoms or molecules, labeled as *A* and *B*, with each of them described by a set of unperturbed energy levels E_i^A and E_j^B . If systems *A* and *B* are brought together, so that there is an overlap between their electronic orbitals, then to second order with respect to the orbital overlap, the interactions between the two systems are pairwise additive over the pairs of those electronic states or orbitals. Each pair interaction can be described through formation of bonding and an-

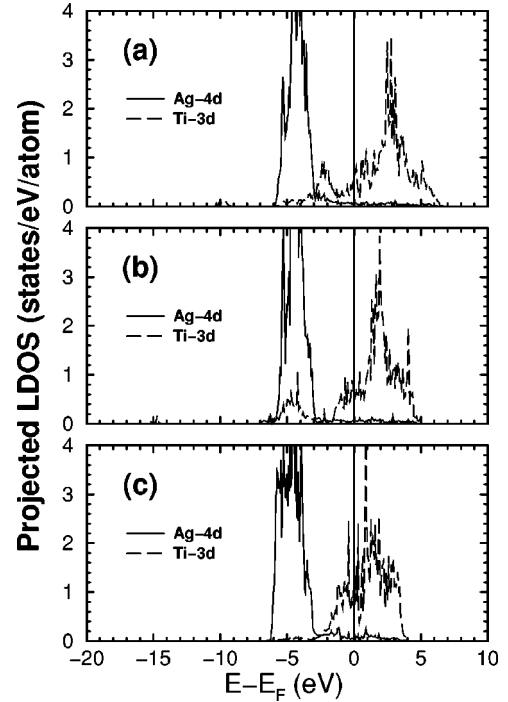


FIG. 15. The electronic LDOS projected onto atomic orbitals of the interface Ag and Ti atoms at Ag(001)/TiC(001) (a) and Ag(001)/TiN(001) (b) with interface C(N) vacancies, compared to those atoms at Ag(001)/Ti(001) (c). The interface structures are like in Fig. 1. All the structures are relaxed.

tibonding states below and above the unperturbed energy levels, respectively. The electrons of the original levels E_i^A and E_j^B now occupy the newly formed bonding and antibonding states. If both the bonding and antibonding states are filled, then the interaction has repulsive character, as the antibonding combination goes up in energy more than the bonding goes down.⁵⁹ If the bonding state is filled and the antibonding state is empty, then the interaction is attractive, and its contribution to the total *A-B* interaction energy is

$$\Delta E \approx \frac{|H_{ij}|^2}{|E_i^A - E_j^B|}, \quad H_{ij} \ll |E_i^A - E_j^B|. \quad (8)$$

Here $|H_{ij}|$ is the coupling matrix element, which is governed by the overlap of the E_i^A and E_j^B electronic orbitals.

In our qualitative analysis of Ag-Ti bonding in Ag/Ti(C,N) systems, we take as unperturbed energy levels the Ag-*d* and Ti-*d* bands of the surface atoms of Ag(001) and Ti(C,N)(001) of Ti(001) free slabs [see Fig. 16]. As pointed out in, e.g., Ref. 49, unrelaxed systems are typically a more suitable choice for the analysis of the nature of bonding.

When estimating the positions of the Ti *d*-band center for TiC and TiN, we neglect the LDOS peaks from the C-Ti *p-d* bonding states, as we can expect that those states are localized along the TiC bonds and won't have significant overlap with the Ag states at an Ag/Ti(C,N) interface.

The positions and behaviors of the Ag-*d* and Ti-*d* LDOS are not drastically modified when Ag/Ti(C,N) or Ag/Ti interfaces are formed (Fig. 17), so the above perturbation theory

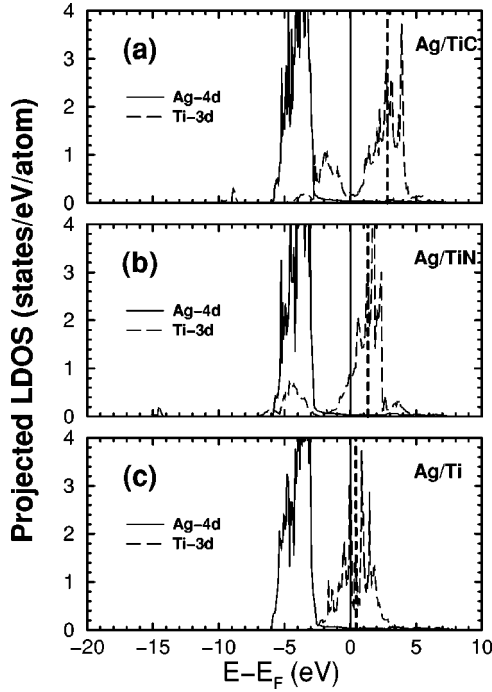


FIG. 16. The electronic LDOS projected onto atomic orbitals of the surface Ag and Ti atoms at: (a) Ag(001) and TiC(001) separated slabs; (b) Ag(001) and TiN(001) separated slabs; (c) Ag(001) and fcc Ti(001) separated slabs. The slabs are taken as truncated bulks (unrelaxed). The dot-dashed vertical lines show the estimated position of the Ti- d energy-band centers. Note that Ag slabs in (a)–(c) differ in their strain, as they match different substrates.

description should be a reasonable approximation. As the Ag d states are practically fully below the Fermi level and the partially occupied Ti d states are mainly above the Fermi level, we can expect that Ag-Ti bonding states should be below the Fermi level, while the antibonding states will mostly appear above the Fermi level.

A comparison of the LDOS features for metal-over-Ti structures of Ag/Ti(C,N) or Ag/Ti interfaces (Fig. 17) and the corresponding separated slabs (Fig. 16) reveals the LDOS peaks near the top of Ti d -band that are likely to correspond to the Ag-Ti antibonding states (marked with arrows in Fig. 17). The interface induced modifications of the Ag- d LDOS mainly affect the energy interval near the bottom of the Ag- d band, which can be attributed to the formation of the bonding states. For example, the Ag- d LDOS peak around -5.5 eV for the Ag/Ti interface [Fig. 17(c)] can be expected to be from the Ag-Ti bonding states.

The described perturbation-theory interaction picture allows us to understand the trends in the Ag-Ti bonding when going from Ag/TiC to Ag/TiN and to Ag/Ti. As an indicator of the Ag-Ti bonding strength we take the value of the ideal work of separation, W_{sep} , for unrelaxed Ag-over-Ti structures [Fig. 1(b)]. The corresponding W_{sep} values are 0.30, 0.69, and 1.68 J/m² for Ag/TiC, Ag/TiN, and Ag/Ti systems, respectively. That is, the Ag-Ti bonding strength should be increasing from Ag/TiC to Ag/TiN and Ag/Ti. To explain this trend let us notice that in the series of Ag/TiC, Ag/TiN, and Ag/Ti the Ti d band moves closer in energy to the Ag d band

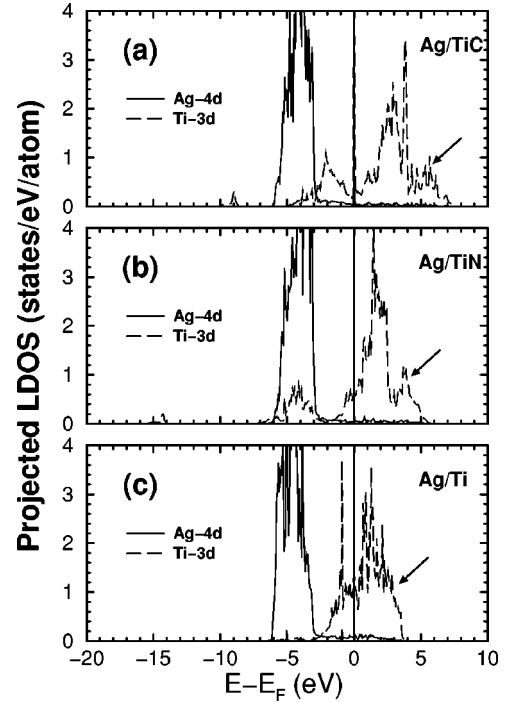


FIG. 17. The electronic LDOS projected onto atomic orbitals of the interface Ag and Ti atoms for metal-over-Ti [Fig. 1(b)] structures of Ag(001)/TiC(001) (a), Ag(001)/TiN(001) (b), and Ag(001)/Ti(001) (c). The Ag, TiC, TiN, and Ti slabs are kept as truncated bulk (unrelaxed structures). The arrows point at the LDOS features that are expected to correspond to Ag-Ti antibonding states.

(Fig. 16). This implies the decreasing value of the denominator in expression (8), and hence the increasing energy gain ΔE from the Ag-Ti bonding.

When the number of C(N) neighbors of the Ti atoms is reduced, for example at Ti(C,N)(011) or Ti(C,N)(111) surfaces or by introducing C(N) vacancies (Fig. 15), the Ti d band becomes closer in energy to the Ag d band, which leads to stronger Ag-Ti bonds.

VIII. CONCLUSIONS

In conclusion, a number of important aspects of wetting of TiC and TiN by liquid metals have been analyzed at the microscopic level, using first-principles density-functional computational experiments in the framework of the generalized gradient approximation. The analysis is based on total-energy and electronic structure calculations with the plane-wave pseudopotential method applied to an extensive set of model interface system.

The large variations of the wetting angles for Cu and Ag on TiC and TiN from experiment to experiment are rationalized in terms of the relative contributions of the metal-over-Ti and metal-over-C(N) local atomic coordinations at the interface. In particular, when poor wetting is observed, the experimental trends correlate well with the adhesion at metal-over-Ti type model interfaces. This implies a suppressed contribution of the metal-over-C(N) configurations, which can be caused by the substrate surface contamination or other experimental factors. The situation of wetting, or

near the nonwetting to wetting transition, corresponds to a balanced mixture of metal-over-Ti and metal-over-C(N) local configurations.

Based on our results for Ag(001)/Ti(C,N)(001), Ag(011)/Ti(C,N)(011), and Ag(111)/Ti(C,N)(111), we analyze the dependence of the interface energetics on the interface orientation relationship. According to the calculations, there are overlaps between the regions of interface energy values for different orientation relationships. This suggests a possibility for a coexistence of different faces of the Ti(C,N) particles in an Ag melt. This is consistent with the experimental observation that Ti(C,N) particles can be changing their shapes.

The key factor in the structural and orientational dependence of the interface energetics is the number of metal-C(N) and metal-Ti bonds per interface area. An important contribution to the orientation dependence of the interface adhesion is also the strength of the Ag-Ti bonding, which is controlled by the number of the nearest C(N) neighbors around the interface Ti atoms. The less C(N) neighbors a Ti atom has, the stronger the Ag-Ti bonding is. This is in line with the noticeably higher strength of the Ag-Ti bonds at Ag/Ti than at Ag/Ti(C,N).

For the energetically favorable structures of Ag/Ti(C,N) interfaces, there is a noticeable increase both of work of separation and interface energy in the series of (001)|| (001), (011)|| (011), and (111)|| (111). For a given interface orientation, the most energetically favorable structures are the ones that have maximal total number of Ag-C(N) and Ag-Ti bonds per interface Ag atom.

In agreement with the experimental fact of better wettability of hypostoichiometric Ti(C,N), our calculations for an Ag/Ti(C,N) model system show that C(N) vacancies tend to strengthen the interface adhesion. It is mainly vacancies of the first two Ti(C,N)(001) surface layers that have any noticeable effect on the Ag/Ti(C,N) interface adhesion. The magnitude of the vacancy contribution to the ideal work of separation is consistent with the difference between the work of separation for Ag/Ti(C,N) and Ag/Ti cases.

The role of Ti and Al additives in the metal melt is analyzed. The calculated energetics of Ti/Ti(C,N)(001) model systems indicate that the interface segregation of Ti in the melt can have a noticeable positive effect on the metal/Ti(C,N)(001) interface adhesion. This agrees with known experimental facts. The results for Al/Ti(C,N)(001) interfaces show that the effects of Al segregation should not be of much significance.

The behaviors of the electron density and local density of states indicate that the nature of the metal-C(N) bonding across the Cu,Ag,Au/Ti(C,N)(001) interfaces is similar to what was previously reported for Co/Ti(C,N)(001) and Co/WC(001). The analysis of the electron density distribution suggests that a change in the interface orientation should not introduce any qualitative changes in the nature of the interface metal-C(N) bonds.

The systematics of the calculated work of separation, in particular, the differences between bonding to Cu, Ag, and Au, as well as between the metal/TiC and metal/TiN adhesion, correlates well with the noticeable variations of the charge-density values at the interface metal-C(N) bonds. For the same metal, metal-C(N) bonding at the metal/TiC interfaces is noticeably stronger than at metal/TiN ones. This is due to the fact that the more tightly bound electrons of N in TiN create weaker metal-C(N) *p-d* bonds across the interface than the *C-p* electrons in TiC. A similar effect is that the more tightly bound *d*-band states in Ag lead to weaker adhesion at the Ag/Ti(C,N)(001) interfaces, as compared to the Cu/Ti(C,N)(001) or Au/Ti(C,N)(001) ones.

ACKNOWLEDGMENTS

This work was partially supported by the Swedish Foundation for Strategic Research (SSF) via the Materials Consortia No. 9 and ATOMICS. Allocation of computer time at the UNICC facilities at Chalmers University of Technology and at the National Supercomputer Center at Linköping University is gratefully acknowledged.

*Present address: National Renewable Energy Laboratory, Golden, Colorado 80401.

¹O.M. Akselsen, *J. Mater. Sci.* **27**, 1989 (1992).

²H.E. Exner, *Int. Met. Rev.* **24**, 149 (1979).

³J. Gurland, *Int. Met. Rev.* **33**, 151 (1988).

⁴J.G. Li, *Ceram. Int.* **20**, 391 (1994).

⁵X.B. Zhou and J.T.M.D. Hosson, *Acta Mater.* **44**, 421 (1996).

⁶C. Iwamoto and S.-I. Tanaka, *Acta Mater.* **46**, 2381 (1998).

⁷C. Iwamoto, H. Ichinose, and S.-I. Tanaka, *Philos. Mag. A* **79**, 85 (1999).

⁸C. Rada, B. Drevet, and N. Eustathopoulos, *Acta Mater.* **48**, 4483 (2000).

⁹T.P. Swiler and R.E. Loehman, *Acta Mater.* **48**, 4419 (2000).

¹⁰E. Saiz, R.M. Cannon, and A.P. Tomsia, *Acta Mater.* **48**, 4449 (2000).

¹¹L. Ramqvist, *Int. J. Powder Metall.* **1**, 2 (1965).

¹²J.G. Li, *Ceram. Trans.* **35**, 103 (1993).

¹³P. Xiao and B. Derby, *Acta Mater.* **44**, 307 (1996).

¹⁴N. Froumin, N. Frage, M. Polak, and M.P. Dariel, *Acta Mater.* **48**, 1435 (2000).

¹⁵N. Froumin, N. Frage, M. Polak, and M.P. Dariel, *Scr. Mater.* **37**, 1263 (1997).

¹⁶G. Levi, M. Bamberger, and W.D. Kaplan, *Acta Mater.* **47**, 3927 (1999).

¹⁷M.W. Finnis, *J. Phys.: Condens. Matter* **8**, 5811 (1996).

¹⁸S.V. Dudiy, J. Hartford, and B.I. Lundqvist, *Phys. Rev. Lett.* **85**, 1898 (2000).

¹⁹S.V. Dudiy and B.I. Lundqvist, *Phys. Rev. B* **64**, 045403 (2001).

²⁰S.V. Dudiy, *Surf. Sci.* **497**, 171 (2001)

²¹M. Christensen, S. Dudiy, and G. Wahnström, *Phys. Rev. B* **65**, 045408 (2002).

²²D.J. Siegel, L.G. Hector, Jr., and J.B. Adams, *Phys. Rev. B* **65**, 085415 (2002).

²³D.J. Siegel, L.G. Hector, Jr., and J.B. Adams, *Surf. Sci.* **498**, 321 (2002).

²⁴D.J. Siegel, L.G. Hector, Jr., and J.B. Adams, *Acta Mater.* **50**, 605 (2002).

²⁵P. Hohenberg and W. Kohn, *Phys. Rev.* **136**, B864 (1964).

²⁶W. Kohn and L. Sham, *Phys. Rev.* **140**, A1133 (1965).

- ²⁷R.O. Jones and O. Gunnarsson, *Rev. Mod. Phys.* **61**, 689 (1989).
- ²⁸J.P. Perdew, J.A. Chevary, S.H. Vosko, K.A. Jackson, M.R. Pederson, D.J. Singh and C. Fiolhais, *Phys. Rev. B* **46**, 6671 (1992).
- ²⁹M.C. Payne, M.P. Teter, D.C. Allan, T.A. Arias, and J.D. Joannopoulos, *Rev. Mod. Phys.* **64**, 1045 (1992).
- ³⁰G. Kresse and J. Furthmüller, *Phys. Rev. B* **54**, 11 169 (1996).
- ³¹G. Kresse and J. Hafner, *Phys. Rev. B* **49**, 14 251 (1994).
- ³²G. Kresse and J. Hafner, *Phys. Rev. B* **48**, 13 115 (1993).
- ³³G. Kresse and J. Hafner, *Phys. Rev. B* **47**, 558 (1993).
- ³⁴G. Kresse and J. Furthmüller, *Comput. Mater. Sci.* **6**, 15 (1996).
- ³⁵D. Vanderbilt, *Phys. Rev. B* **41**, 7892 (1990).
- ³⁶G. Kresse and J. Hafner, *J. Phys.: Condens. Matter* **6**, 8245 (1994).
- ³⁷P. Pulay, *Chem. Phys. Lett.* **73**, 393 (1980).
- ³⁸H.J. Monkhorst and J.D. Pack, *Phys. Rev. B* **13**, 5188 (1976).
- ³⁹M. Methfessel and A.T. Paxton, *Phys. Rev. B* **40**, 3616 (1989).
- ⁴⁰P.E. Blöchl, O. Jepsen, and O.K. Andersen, *Phys. Rev. B* **49**, 16 223 (1994).
- ⁴¹F.D. Murnaghan, *Proc. Natl. Acad. Sci. U.S.A.* **30**, 244 (1944).
- ⁴²P.H.T. Philipsen and E.J. Baerends, *Phys. Rev. B* **61**, 1773 (2000).
- ⁴³M. Asato, A. Settels, T. Hoshino, T. Asada, S. Blügel, R. Zeller, and P.H. Dederichs, *Phys. Rev. B* **60**, 5202 (1999).
- ⁴⁴L. Vitos, A.V. Ruban, H.L. Skriver, and J. Kollár, *Surf. Sci.* **411**, 186 (2001).
- ⁴⁵A. Khein, D.J. Singh, and C.J. Umrigar, *Phys. Rev. B* **51**, 4105 (1995).
- ⁴⁶M. Körling and J. Häglund, *Phys. Rev. B* **45**, 13 293 (1992).
- ⁴⁷R. Ahuja, O. Eriksson, J.M. Wills, and B. Johansson, *Phys. Rev. B* **53**, 3072 (1996).
- ⁴⁸C. Stampfl, W. Mannstadt, R. Asahi, and A.J. Freeman, *Phys. Rev. B* **63**, 155106 (2001).
- ⁴⁹I.G. Batirev, A. Alavi, M.W. Finnis, and T. Deutsch, *Phys. Rev. Lett.* **82**, 1510 (1999).
- ⁵⁰N. Nogi, K. Ogino, A. Mclean, and W.A. Miller, *Metall. Trans. B* **17B**, 163 (1986).
- ⁵¹G.E. Hollox, *Mater. Sci. Eng.* **3**, 121 (1968).
- ⁵²A. Arya and E.A. Carter, *J. Chem. Phys.* **118**, 8982 (2003).
- ⁵³I. Egry, G. Lohoefer, and G. Jacobs, *Phys. Rev. Lett.* **75**, 4043 (1995).
- ⁵⁴S. Zaima, Y. Shibata, H. Adachi, C. Oshima, S. Otani, M. Aono, and Y. Ishizawa, *Surf. Sci.* **157**, 380 (1985).
- ⁵⁵K.E. Tan, M.W. Finnis, A.P. Horsfield, and A.P. Sutton, *Surf. Sci.* **348**, 49 (1996).
- ⁵⁶F. Ernst, *Mater. Sci. Eng., R.* **14**, 97 (1995).
- ⁵⁷Yu.F. Zhukovskii, E.A. Kotomin, P.W.M. Jacobs, and A.M. Stoneham, *Phys. Rev. Lett.* **84**, 1256 (2000).
- ⁵⁸J. Hartford, *Phys. Rev. B* **61**, 2221 (2000).
- ⁵⁹R. Hoffmann, *Rev. Mod. Phys.* **60**, 601 (1988).
- ⁶⁰M.H. Cohen, M.V. Ganduglia-Pirovano, and J. Kudrnovský, *Phys. Rev. Lett.* **72**, 3222 (1994).
- ⁶¹B. Hammer and J.K. Nørskov, *Surf. Sci.* **343**, 211 (1995).